Monomeric sarcosine oxidase: structure of a covalently flavinylated amine oxidizing enzyme

Peter Trickey[1], Mary Ann Wagner[2], Marilyn Schuman Jorns[2]* and F Scott Mathews[1]*

Background: Monomeric sarcosine oxidases (MSOXs) are among the simplest members of a recently recognized family of eukaryotic and prokaryotic enzymes that catalyze similar oxidative reactions with various secondary or tertiary amino acids and contain covalently bound flavins. Other members of this family include heterotetrameric sarcosine oxidase, *N*-methyltryptophan oxidase and pipecolate oxidase. Mammalian sarcosine dehydrogenase and dimethylglycine dehydrogenase may be more distantly related family members.

Results: The X-ray crystal structure of MSOX from *Bacillus* sp. *B-0618*, expressed in *Escherichia coli*, has been solved at 2.0 Å resolution by multiwavelength anomalous dispersion (MAD) from crystals of the selenomethionine-substituted enzyme. Fourteen selenium sites, belonging to two MSOX molecules in the asymmetric unit, were used for MAD phasing and to define the local twofold symmetry axis for electron-density averaging. The structures of the native enzyme and of two enzyme–inhibitor complexes were also determined.

Conclusions: MSOX is a two-domain protein with an overall topology most similar to that of D-amino acid oxidase, with which it shares 14% sequence identity. The flavin ring is located in a very basic environment, making contact with sidechains of arginine, lysine, histidine and the N-terminal end of a helix dipole. The flavin is covalently attached through an 8α–S-cysteinyl linkage to Cys315 of the catalytic domain. Covalent attachment is probably self-catalyzed through interactions with the positive sidechains and the helix dipole. Substrate binding is probably stabilized by hydrogen bonds between the substrate carboxylate and two basic sidechains, Arg52 and Lys348, located above the *re* face of the flavin ring.

Addresses: [1]Department of Biochemistry and Molecular Biophysics, Washington University School of Medicine, 660 S. Euclid Ave, St Louis, MO 63110, USA and [2]Department of Biochemistry, MCP-Hahnemann School of Medicine, 2900 Queen Lane, Philadelphia, PA 19129 USA.

*Corresponding authors.
E-mail: jornsm@auhs.edu
mathews@biochem.wustl.edu

Key words: amine oxidation, covalent flavinylation, enzyme mechanism, flavoprotein oxidase, X-ray crystallography

Received: 9 November 1998
Revisions requested: 4 December 1998
Revisions received: 23 December 1998
Accepted: 5 January 1999

Published: 4 March 1999

Structure March 1999, 7:331–345
http://biomednet.com/elecref/0969212600700331

 ISSN 0969-2126

Introduction

Monomeric sarcosine oxidases (MSOXs) are among the simplest members of a recently recognized family of prokaryotic and eukaryotic enzymes that contain covalently bound flavin and catalyze similar oxidation reactions with various secondary or tertiary amino acids [1–3] (M Eschenbrenner and MSJ, unpublished results; P Khanna and MSJ, unpublished results). Other enzymes in this family include heterotetrameric sarcosine oxidases (TSOXs), *N*-methyltryptophan oxidase (MTOX) and pipecolate oxidase (PIPOX). Dimethylglycine dehydrogenase (DMGDH) and sarcosine dehydrogenase (SDH) may be more distantly related family members. Except for TSOX, all are monomeric enzymes. MSOX shares ~40% sequence identity with MTOX and ~30% identity with PIPOX [2]. MSOX also exhibits ~20–25% sequence identity with the β subunit of TSOX [1] and with the N-terminal half of rat liver DMGDH [4] and human SDH (M Eschenbrenner and MSJ, unpublished results).

MSOX and TSOX are induced in various soil microorganisms upon growth with sarcosine as a source of carbon and energy [5]. The *Escherichia coli* gene encoding MTOX was isolated on the basis of sequence homology with MSOX [3]. The physiological role of MTOX is unknown. PIPOX plays an important role in brain metabolism, where L-pipecolate is synthesized from lysine and acts as a neuromodulator of the GABA receptor complex [6,7]. SDH and DMGDH are mitochondrial enzymes found in the liver that are involved in choline and 1-carbon metabolism [8,9]. SDH is also a key component in the glycine/sarcosine regulatory cycle [10].

MSOX from *Bacillus* sp. *B-0618* has 386 residues, a molecular mass of 43.8 kDa, and an N-terminal ADP-binding motif [11]. The enzyme contains 1 mol of flavin adenine dinucleotide (FAD) that is bound covalently through an 8α–S-cysteinyl linkage to Cys315 (MAW and MSJ, unpublished results). This cysteine residue is conserved in MSOXs

from other bacteria, MTOX and PIPOX. MSOXs catalyze the oxidation of sarcosine (*N*-methylglycine) by molecular oxygen and water to form glycine, formaldehyde and hydrogen peroxide [5] (Equation 1).

$$CH_3NHCH_2COOH + O_2 + H_2O \rightarrow$$

$$HCHO + NH_2CH_2COOH + H_2O_2 \quad (1)$$

Formaldehyde formation is not suppressed in the presence of tetrahydrofolate [12], in contrast to TSOX, DMGDH and SDH, which can catalyze the formation of 5,10-methylenetetrahydrofolate.

In this paper, we show that MSOX is a two-domain protein with an overall topology that is most similar to that of D-amino acid oxidase (DAAO). The flavin ring is attached to Cys315 in the catalytic domain and located in a very basic environment. Active-site residues th-at are likely to bind sarcosine or to assist in its oxidation have been tentatively identified on the basis of the structure of MSOX–inhibitor complexes. These residues are conserved in MSOX from other bacteria, MTOX, PIPOX and the β subunit from TSOX.

Results

Structure determination

The crystal structure of MSOX from *Bacillus* sp. *B-0618* was solved by multiple wavelength anomalous dispersion (MAD) methods [13] at 2.0 Å resolution by the replacement of the seven methionine residues with selenomethionine; electrospray mass spectroscopy showed that all seven methionines were fully substituted. The anomalous and dispersive signals of the selenomethionine crystals were used to identify 14 selenium sites belonging to two MSOX molecules in the asymmetric unit of the monoclinic unit cell (Table 1). These sites were located by difference Patterson methods and used for MAD phasing and to define the local twofold noncrystallographic symmetry (NCS) axis for electron-density averaging. Twofold NCS averaging

Table 1

Diffraction data, phasing statistics and model refinement.

Data set	Native	(Methylthio) acetic acid	Pyrrole-2-carboxylic acid	Edge	Peak	Low	High
Wavelength (Å)	1.54	1.54	1.54	0.9794	0.9792	1.0679	0.9392
Beam/detector	R-Axis IV	R-Axis II	R-Axis IV	APS/SBC	APS/SBC	APS/SBC	APS/SBC
Observations	159,021	166,307	248,407	203,670	229,300	206,125	230,951
Reflections*	49,557	43,804	44,120	49,062	49,012	46,323	49,543
Completeness (%)†	98.6 (81.0)	88.4 (53.6)	89.1 (47.2)	96.9 (64.0)	98.0 (86.8)	92.5 (57.6)	98.4 (87.5)
$R_{sym}H$ (%)†	7.0 (19.4)	8.8 (25.0)	8.3 (33.0)	6.3 (14.0)	6.4 (14.7)	5.6 (15.5)	7.3 (46.5)
$<I/\sigma(I)>$†	11.9 (4.2)	10.3 (2.0)	13.4 (3.8)	10.4 (5.4)	9.7 (6.3)	10.3 (5.6)	5.7 (2.0)
Phasing power‡ (a/c)	–	–	–	4.0/2.64	4.65/2.77	–	1.40/1.38
R_{cullis} § (a/c)	–	–	–	0.38/0.42	0.42/0.50	–	0.98/1.0
R_{cullis} (anomalous)	–	–	–	0.75	0.66	0.98	0.90
Refinement							
R/R_{free} ($F_o > 2\sigma$) (%)	18.0/25.3	19.4/24.4	22.3/27.3	20.3/24.8			
Number of protein atoms	6122	6138	6142	6124			
Number of solvents	206	183	185	232			
Rmsd							
Bond lengths (Å)	0.016	0.016	0.017	0.016			
Bond angles (°)	3.02	3.08	3.17	3.00			
Dihedral angles (°)	26.28	26.45	26.30	26.24			
Improper torsions (°)	1.64	1.53	1.66	1.50			
Rms ΔB (m/m, Å²)¶	2.2	0.7	0.6	0.8			
Rms ΔB (m/c, Å²)¶	2.8	0.8	0.7	1.0			
Rms ΔB (c/c, Å²)¶	3.7	1.0	0.9	1.4			
B factor							
Mainchain (Å²)	25.04	20.66	23.43	21.45			
Sidechain (Å²)	27.86	21.69	24.41	23.17			
Solvent (Å²)	26.17	21.02	24.42	25.62			

*Reflections including both pairs of Friedel-related reflections. †Values in parentheses correspond to the outermost resolution shell 2.03–2.00 Å. †$R_{sym} = \Sigma|I-<I>|/\Sigma<I>$, where I is the reflection intensity and the summation is over all the equivalent measurements including Friedel pairs. ‡Phasing power = $<F_H>/<E>$, where $<F_H>$ and $<E>$ are the root mean square heavy-atom structure-factor and lack of closure, respectively and a/c refers to acentric/centric reflections. §$R_{cullis} = \Sigma||F_{PH}-F_P|-F_H||/\Sigma|F_{PH}-F_H|$, where F_{PH}, F_P and F_H are the structure-factor amplitudes for the heavy-atom derivative, the native protein and the heavy-atom contribution, respectively. ¶Rms difference in B factor for bonded atoms; m/m, m/c and c/c represent mainchain–mainchain, mainchain–sidechain and sidechain–sidechain bonds, respectively.

Figure 1

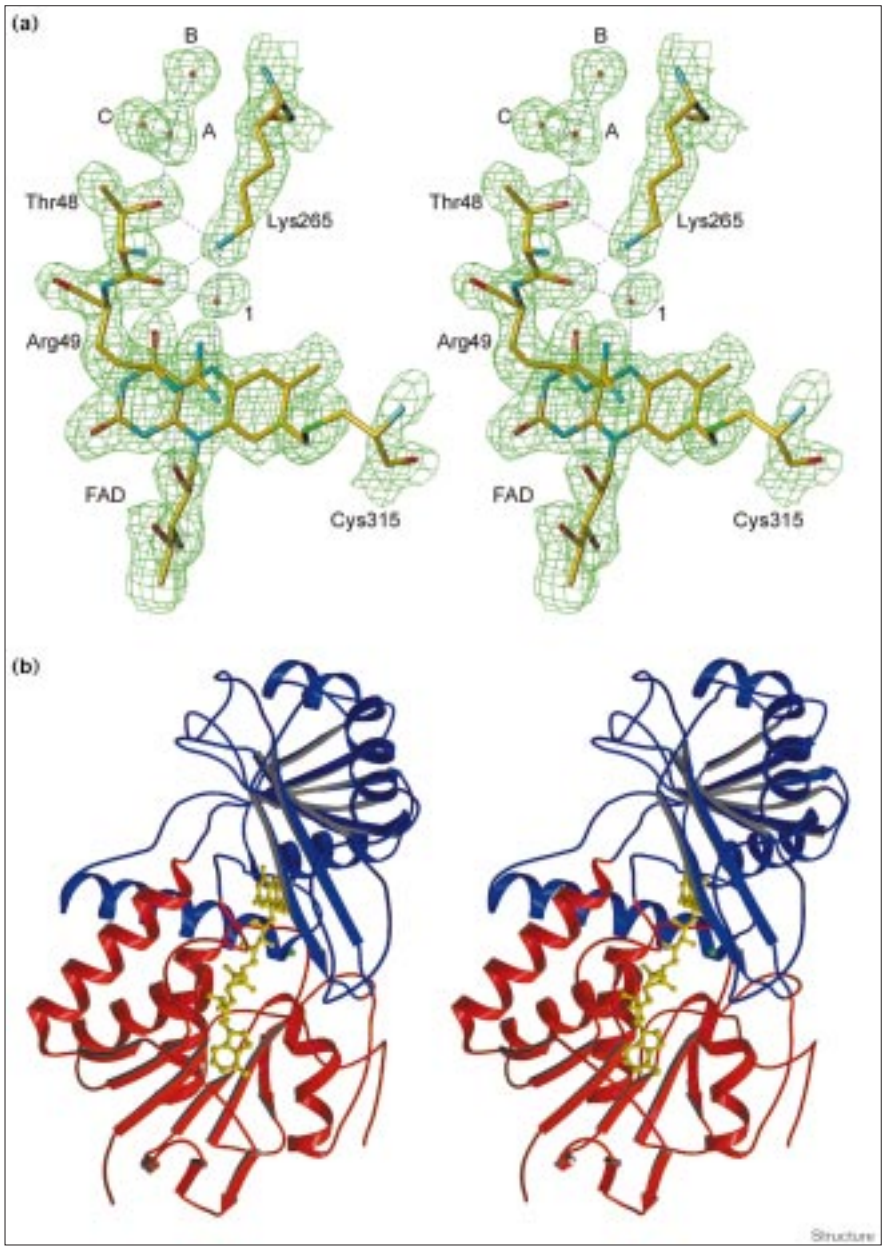

Electron density and protein fold of MSOX. (a) Solvent-flattened and twofold noncrystallographic symmetry averaged MAD electron density showing flavin and its covalent attachment to Cys315 in the selenomethionine structure. Residues Thr48 and Lys265 and four water molecules making up a proton relay system are also indicated. Water molecule 1 is hydrogen bonded to flavin N(5), water molecule A to Thr48 OG and to water molecules B and C, and water molecule B to Gly263 O (not shown). Water molecule C is most accessible to bulk solvent. Water molecules A, B and C are also present in the native and inhibitor-bound complexes of MSOX. Contouring is at 1σ. The figure was generated with the program TURBO-FRODO [59]. (b) Stereoview ribbon diagram of MSOX with the domains distinguished by color: blue, the catalytic domain; red, the FAD-binding domain. FAD is shown in yellow. The figure was generated using the program MOLSCRIPT [61] and rendered using RASTER3D [62,63].

improved the phases, producing a readily interpretable map (Figure 1a). The structures of the native (sulfur-methionine) protein and of two enzyme–inhibitor complexes of the selenomethionine protein were then determined directly by utilizing the refined selenomethionine coordinates for refinement and model-building against the native and inhibitor complex data at 2.0 Å resolution.

The final R factors of the native structure are R = 18.0% and R_{free} = 25.3%, with root mean square deviations (rmsds) in bond lengths and angles of 0.016 Å and 3.02°, respectively. The R factors and rmsds for the three selenomethionine structures are similar to those of the native protein (Table 1). In both subunits of all four structures, the model is truncated at Gln385, because of the lack of electron density for the four C-terminal residues. The average B factors for mainchain and sidechain atoms are 25.0 $Å^2$ and 27.9 $Å^2$, respectively, for both subunits of the native MSOX and are approximately the same for selenomethionine and inhibitor structures (Table 1).

The refined model of MSOX has good geometry according to the program PROCHECK [14]. More than 91% of the amino acids are in the most favored region, and only

Asp47 (average $\phi = 74°$, $\psi = 50°$) in both molecules lies outside of the allowed regions. Asp47 fits the electron density well and forms part of a long coil section between residues 32 and 59 that starts in the FAD domain and ends in the catalytic domain. A sharp turn at Gly46 presumably results in the non-standard ϕ,ψ angles of Asp47. There is one *cis*-proline per molecule (Pro38), which is also in good electron density and is also located in the long coil section between residues 32 and 59.

The final native (sulfur-methionine) structure refinement was performed without NCS restraints in order to determine the differences between the two molecules. The rmsd between the Cα atoms of the two molecules in the asymmetric unit in the unrestrained refinement is 0.3 Å, indicating that they are effectively equivalent, and so no distinction will be made between them in this article. Because of the lack of significant difference between the two molecules in the native structure, weak NCS restraints were maintained in the three selenomethionine structure refinements, giving an average rmsd between the two molecules in each of the asymmetric units of 0.1 Å.

Description of the structure

MSOX is a two-domain protein of the flavoenzyme structural class first observed in *p*-hydroxybenzoate hydroxylase (PHBH) [15] (Figures 1b,2a); its folding topology is shown in Figure 2b. One domain contains a 'classic' FAD-binding motif that is common to the PHBH class and to the glutathione reductase (GR) [16] class of flavoproteins. In MSOX, this motif consists of a five-stranded parallel β sheet flanked on one side by two α helices, αF1 and αF2, preceding strands βF2 and βF3 of the sheet respectively, and by a three-stranded antiparallel β sheet (a 'β meander', strands βF4–βF6) on the other side of the sheet preceding strand βF7. A third and fourth helix (αF3 and αF4) are packed on either side of the sheet near strands βF8 and βF9. The FAD-binding motif is interrupted twice by excursions into domain 2, the 'catalytic' domain, a two-part, eight-stranded and mostly antiparallel β sheet. One part interrupts the flavin-binding motif between strands βF2 and βF3 and comprises three antiparallel β strands (βC1–βC3) interspersed with three α helices. The other part interrupts the motif between strands βF7 and βF9 and comprises five antiparallel β strands (βC4–βC8) and one α helix. The two-part nature of domain 2 is characteristic of the PHBH flavoprotein class. In the GR flavoprotein class, the second domain, a dinucleotide-binding domain closely resembling the FAD-binding domain, occurs as a single excursion interrupting the FAD-binding domain between β strands four and five.

The PHBH class of FAD-binding proteins contains six members whose structures have been determined: PHBH, MSOX, DAAO [17,18], cholesterol oxidase [19], glucose oxidase [20] and phenol hydroxylase [21]. Comparing MSOX with these other family members using the program DALI [22] indicates that MSOX is most similar to DAAO (Figure 2c; 14% sequence identity in 311 equivalent residues, rmsd = 3.1 Å for Cα positions), and that these two proteins form a subfamily of the PHBH structural class. Interestingly, DAAO is the one flavoprotein of the classic FAD-binding motif that lacks the characteristic β meander.

Flavin environment

FAD is bound to MSOX in a manner similar to that of other members of the PHBH class of flavoenzymes, in particular to DAAO. It is in an extended conformation and is almost totally isolated from bulk solvent; this includes the adenosine portion of the molecule which is partially exposed to bulk solvent in many FAD-containing flavoenzymes. The covalent, hydrogen-bonding and electrostatic interactions made by FAD in the enzyme are indicated in Figure 3. These include one covalent bond, 28 hydrogen bonds, of which eight are to solvent molecules, and two helix dipoles. One of the helix dipoles, at the N terminus of αF4, points toward the N(1)–O(2) portion of the flavin ring; the other dipole, at the N terminus of αF1, points toward the pyrophosphate group of FAD. Both of these helix dipole interactions are found in all members of the PHBH and GR classes of FAD-binding proteins, both classes sharing the same FAD dinucleotide-binding motif. The αF1 helix serves to partially neutralize the double-negative charge on the pyrophosphate group and the αF4 helix helps to stabilize the electrophilic character of the flavin ring and the anionic forms of the hydroquinone and semiquinone. The latter may also help promote covalent flavinylation of certain members of these two flavoprotein classes (see the Discussion section).

There are several notable interactions that distinguish the environment of FAD in MSOX from that in DAAO (the FAD-containing enzyme that is most closely related to MSOX) and give the FAD environment a distinctively basic character (Figure 4a). The flavin O(2) of MSOX is hydrogen bonded to a lysine sidechain (Lys348) and the ribityl hydroxyl O(2*) is linked to the sidechain of Arg49 (Figure 3). In DAAO, O(2) is hydrogen bonded to a threonine sidechain and O(2*) has no ligand. In MSOX, Arg49 is situated below the flavin ring (on the *si* face) and its sidechain is in van der Waals contact with the flavin ring (Figure 1a). The N(5) atom of the flavin ring is hydrogen bonded to two water molecules. One of these (on the *re* face) is displaced upon binding of inhibitors (*vide infra*). The other (on the *si* face) is not displaced. It appears to be part of a proton relay system (PRS) that extends from N(5) of FAD to the protein surface above the *si* face of the flavin ring via a network of hydrogen bonded components. The PRS involves Thr48, Lys265 and four water molecules. Water molecule 1 is hydrogen bonded to flavin N(5), the carbonyl oxygen of Thr48 and the ε-amino group of Lys265 (Figure 1a). The other three water molecules are accessible to bulk solvent.

Figure 2

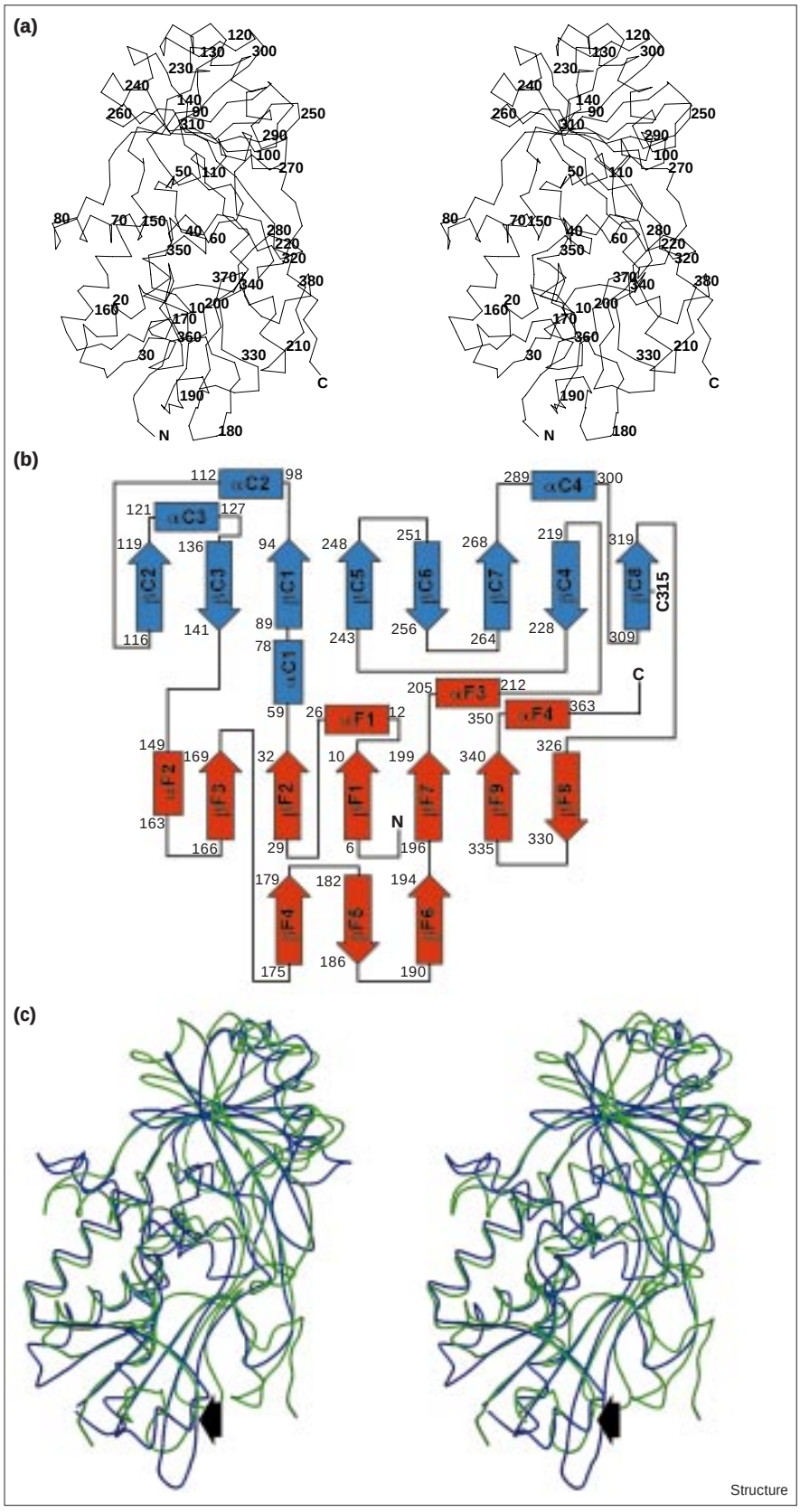

Protein fold and topology of MSOX. (a) Stereoview Cα trace of one molecule of the MSOX structure. Every tenth Cα atom is labeled. The figure was generated with TURBO-FRODO [59]. (b) A topological diagram of the MSOX structure; β strands are shown as arrows and α helices as rectangles. The strands and helices are colored as in Figure 1b and labeled F for FAD-binding domain and C for catalytic domain; their starting and ending residues are indicated, as is the covalent flavin attachment site, C315. (c) A stereo plot of the superposition of Cα traces of DAAO (dark blue) and MSOX (green). The position of the β meander, present in MSOX but absent in DAAO, is indicated by an arrow. The figure was generated using MOLSCRIPT [61] and rendered using RASTER3D [62,63].

Figure 3

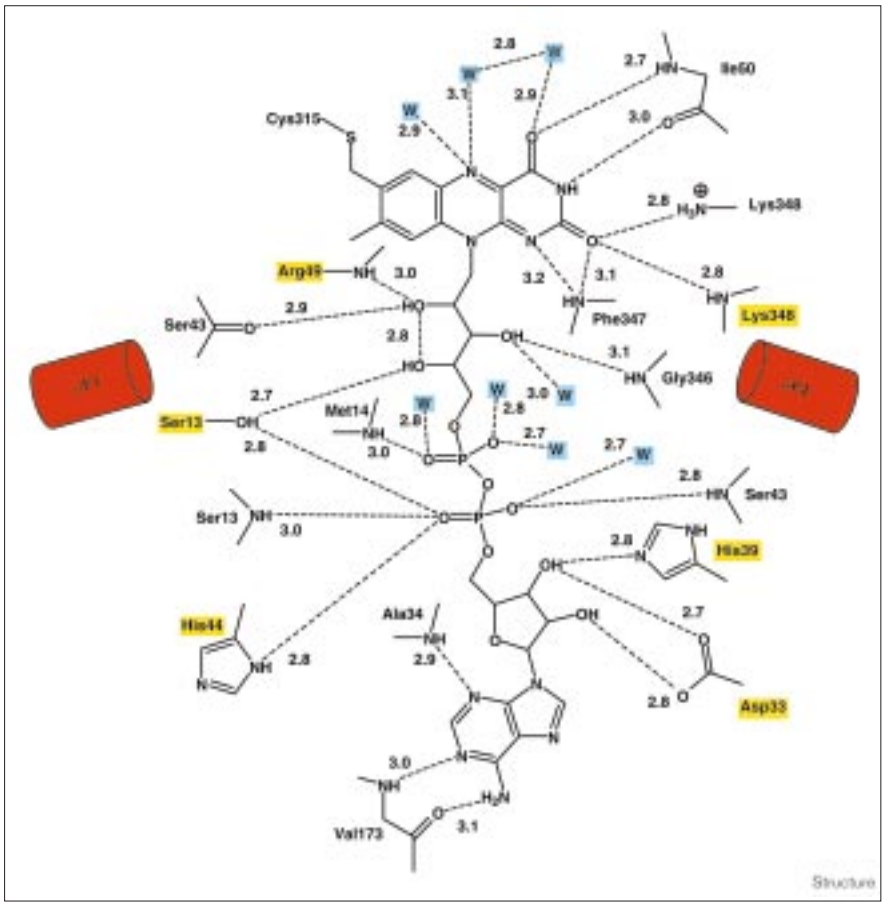

Protein and solvent interactions of FAD. A schematic representation of the FAD–MSOX interactions in the native structure, identifying residues involved in hydrogen bonding to the cofactor. Sidechain interactions are labeled in yellow and water molecules in blue. The locations of two helices that form electrostatic interactions with FAD are indicated in red. Distances are indicated in Ångstroms.

In DAAO there is no PRS because N(5) is hydrogen bonded to a peptide amide group and the *si* face of the flavin ring is in van der Waals contact with a polypeptide chain. In MSOX, O(3*) of the ribityl sugar is in contact with a peptide amide group and a solvent molecule. In DAAO, O(3*) forms a hydrogen bond with a peptide carbonyl. In both proteins, the remainder of the FAD atoms, from O(4*) to the adenine ring, make very similar protein contacts.

There are no acidic residues in the region surrounding the isoalloxazine ring, only neutral or basic residues (His45, His269, His345, Lys265, Lys348, Arg49 and Arg52) (Figure 4b). His45 ND1 is 4.7 Å from Cys315 SG and 6.5 Å from the 8α-methyl covalent attachment site. In addition to the basic residues, there are a number of tyrosine residues near the flavin ring (Tyr55, Tyr61, Tyr254 and Tyr317). The highly basic nature of the environment of the flavin ring in MSOX is unusual among flavoproteins. The sea of nearby positive residues and the positive end of the αF4 helix dipole, which starts at Phe347, may cause a positive shift in the flavin redox potential. Although it has not yet been measured directly, the redox potential of the flavin in MSOX is likely to be high because it is reducible with thiols (MAW and MSJ, unpublished results), a feature observed with high potential flavins in model studies [23].

Inhibitor-bound structures

(Methylthio)acetic acid (MTA) and pyrrole-2-carboxylic acid (PCA) are both competitive inhibitors of MSOX (K_d = 2.6 mM and 1.3 mM, respectively; MAW and MSJ, unpublished results). Both inhibitors also form charge transfer species with MSOX, presumably due to the close proximity of the electron-rich sulfur of MTA or the conjugated pyrrole ring of PCA to the electron-accepting flavin ring. The charge transfer band of the MTA complex is intense (λ_{max} = 532 nm, $\varepsilon_{532} = 6.9 \times 10^3\ M^{-1}\ cm^{-1}$) and gives the protein a pink color; the charge transfer band of the PCA complex is about one-third as intense (λ_{max} = 608 nm, $\varepsilon_{608} = 2.1 \times 10^3\ M^{-1}\ cm^{-1}$).

Crystals of MSOX were soaked in the presence of the inhibitors in order to determine their binding mode and to gain insight into the binding of the substrate, sarcosine. Crystals of the selenomethionine-substituted enzyme were used due to a scarcity of crystals of the native enzyme. Inhibitor concentrations that were about sevenfold in

Figure 4

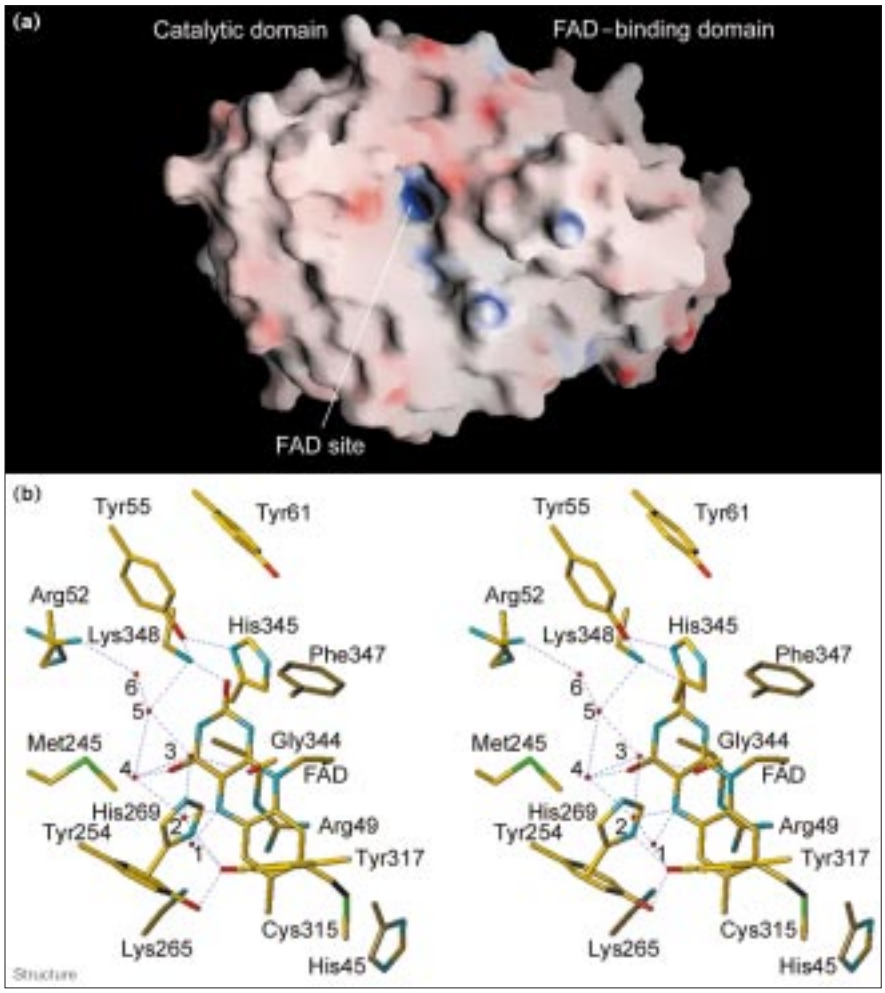

Protein surface potential and environment of FAD. (a) A molecular surface drawing of native MSOX colored according to electrostatic potential (blue, positive; red, negative), showing the cleft to the active site. The figure was generated with GRASP [64]. (b) A stereo plot of the flavin environment. Three basic sidechains (His45, Arg49 and Lys265) lie below the flavin ring, on the *si* face, and four (Arg52, His345, His269 and Lys348) are above the ring, on the *re* face. Water molecules 1 and 2 are hydrogen bonded to the flavin N5. There are also four tyrosine sidechains (Tyr55, Tyr61, Tyr254 and Tyr317) and five water molecules (waters 2–6) located above the flavin ring. The latter are displaced by binding of the inhibitors (methylthio)acetic acid (MTA) and pyrrole-2-carboxylic acid (PCA). The figure was generated with TURBO-FRODO [59].

excess of their K_d were used (see Materials and methods section). The MTA-treated crystals became pink in color but the PCA-treated crystals remained yellow. The selenomethionine form of the inhibitor-bound enzyme was found to be spectrally indistinguishable from the native enzyme and exhibited similar K_d values for PCA and MTA. Difference Fourier analysis of the inhibitor-bound crystals, followed by simulated annealing refinement and model building, led to the unambiguous placement of the inhibitors in the active site.

Both inhibitors are bound to the *re* face of the flavin ring, with one carboxylate oxygen hydrogen bonded to the sidechain of Lys348. On binding of the inhibitors, four solvent molecules are displaced, and the sidechain of Arg52 moves into the active site forming a second hydrogen bond with the inhibitor carboxylates (Figure 5a). The movement of Arg52 displaces a fifth solvent molecule and a new solvent molecule occupies the position vacated by Arg52. This movement also induces a large motion of a loop region consisting of residues Gly56 to Glu60 that results in the movement of Glu57 into the active site and in the formation of a hydrogen bond between its sidechain and that of Arg52, preventing additional solvent from accessing the active site. The movement of the loop breaks a hydrogen bond between Arg59 O and Tyr61 N, but two new hydrogen bonds are formed. The sidechain of the surface residue Glu103 moves into a hydrogen-bonding position with the mainchain of Arg59, and the sidechain of Arg59 flips over also to form a hydrogen bond with Glu103. Glu60 moves across to occupy the space vacated by the mainchain of Gly58 and Arg59.

The residues adjacent to the loop, Tyr55 and Tyr61, are anchored into positions that are almost identical to those in the native structure by steric restraints in the active site and by hydrogen bonds to His345 and Lys348, and to His324, respectively. In the native structure, this loop region is disordered, with its atoms having high B factors (>50 Å^2) and lying in weak electron density. The loop

Figure 5

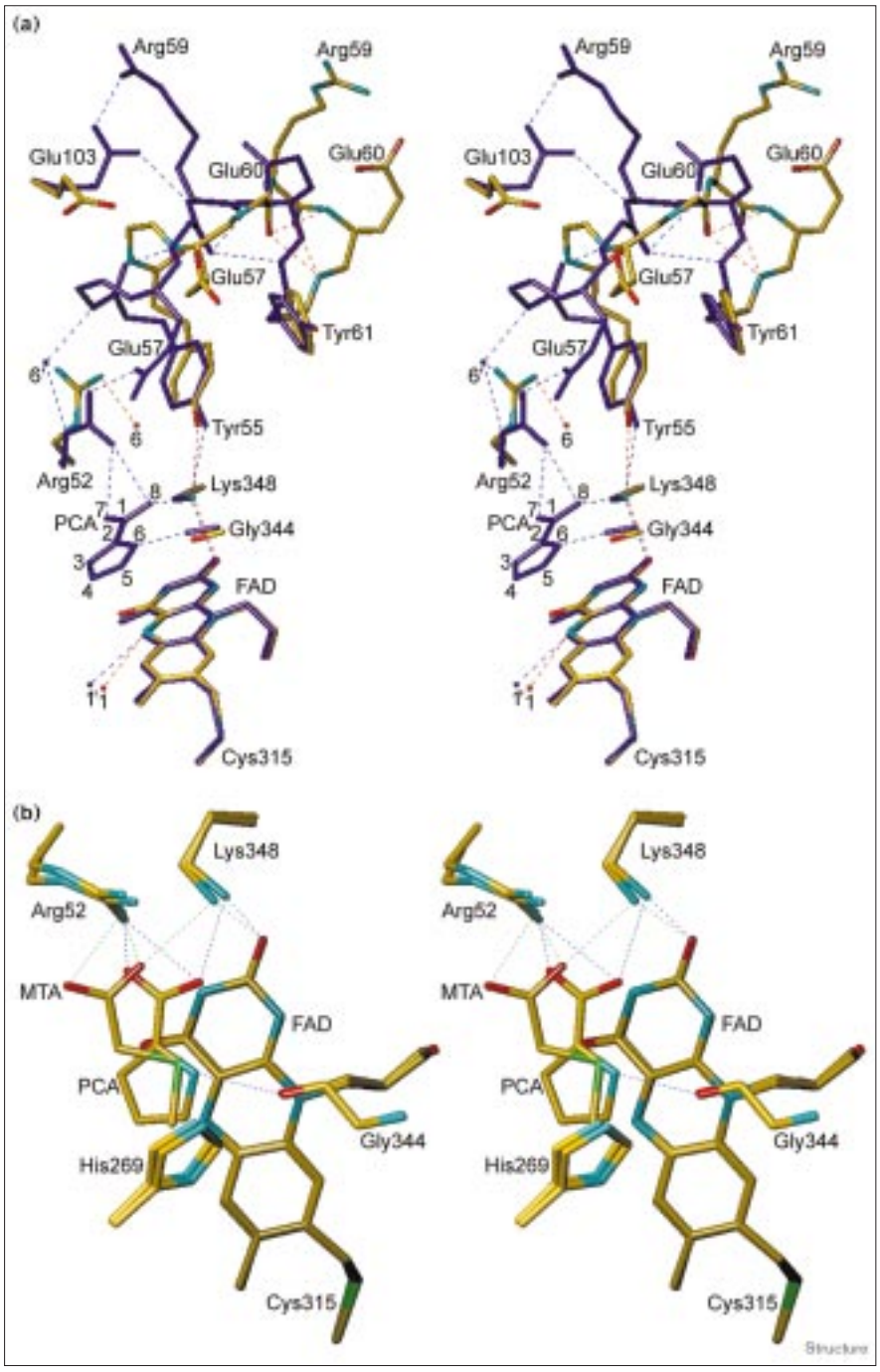

Diagrams showing the conformational change and active-site environments of the inhibitor-soaked crystals. (a) Stereo plot of the active site showing the conformational change that occurs on binding the inhibitor PCA. The native structure is shown in atomic colors (C, yellow; O, red; N, blue; S, green) and the PCA-bound structure is in violet. The largest structural changes occur for the mainchain and sidechain of the loop residues between Tyr55 and Tyr61 and the sidechain of Arg52 (see text). Water sites 1, 6 and 1′, 6′ are alternate sites in the native and inhibitor-bound structures, respectively. The sites for water 6 and Arg52 exchange positions on binding PCA. The numbering scheme for PCA is indicated, atoms 1–5 being carbon, atom 6 the pyrrole nitrogen and atoms 7 and 8 the carboxylate oxygens. The figure was generated with TURBO-FRODO [59]. (b) Stereo plot of the active site comparing the binding of the two inhibitors, PCA and MTA, bound above the *re* face of the flavin ring. The numbering scheme for MTA is CH_3(4)-S(3)-CH_2(2)-C(1)O_2(5,6)$^-$; O(6) is hydrogen bonded to both Lys348 and Arg52 whereas O(5) is hydrogen bonded only to Arg52. See Figure 5a for the PCA numbering scheme. The figure was generated with TURBO-FRODO [59].

forms part of the cleft leading from the surface to the active site of the enzyme. The flexibility of this loop region might aid substrate binding and product release. In the inhibitor structures, this loop is well ordered with normal B factors (<35 Å^2) and strong electron density. The movement of this loop in the inhibitor-bound complexes is accompanied by the shielding of the positive molecular surface potential at the FAD site exhibited by the native enzyme (Figure 4a). This suggests that Arg52 and the loop region from residues Gly56 to Glu60 acts as a switch for the active site in which the loop is flexible in the absence of substrate and then, when Arg52 coordinates to the substrate, the loop is locked into a fixed conformation.

The interaction of MTA and PCA with the active site of MSOX is shown in Figure 5b. PCA is nearly planar and lies

parallel to the plane of the flavin ring, with its pyrrole ring about 3.1 Å above atoms O(4), C(4), C(4a) and N(5) of the flavin ring. PCA interacts with the protein in three places: one carboxylate oxygen (O(8), see numbering scheme in Figure 5a) is hydrogen bonded to Lys348 NZ (2.7 Å) and to Arg52 NH1 (3.2 Å); the other carboxylate oxygen (O(7)) is hydrogen bonded to Arg52 NH1 (2.9 Å); the pyrrole nitrogen (N(6)) is hydrogen bonded to the carbonyl oxygen Gly344 O (2.7 Å). Interestingly, the amino group of *o*-aminobenzoate (OAB), a substrate analog of DAAO, forms a hydrogen bond in the DAAO–OAB complex to the carbonyl oxygen of Gly313, which is located in an equivalent position to Gly344 of MSOX [24]. MTA is less planar than PCA, with atoms C(2), S(3) and C(4) about 3.1–3.2 Å above the flavin ring atoms O(4), C(4), C(4a) and N(5). The carboxylate of MTA is shifted somewhat from that of PCA so that one oxygen (O(6), see numbering scheme in the legend to Figure 5b) is hydrogen bonded to both Lys348 NZ and Arg52 NH1 (2.9 Å each) and the other (O(5)) is farther from Arg52 NH1 (3.3 Å). The sulfur atom is incapable of forming a hydrogen bond to Gly344 O and is 3.1 Å from it.

The two inhibitor complexes reveal a significant deviation in their modes of binding, as shown by the superposition of their active sites (Figure 5b). The PCA inhibitor probably provides a better model for binding the sarcosine substrate of MSOX than MTA. Sarcosine would be likely to form the same three interactions with the protein as PCA and its binding can be simulated simply by deleting atoms C(3) and C(4) of the pyrrole ring. Although MTA has the same number of atoms as sarcosine, the greater sulfur-to-carbon bond distance (1.8 Å), tighter bond angle at the sulfur (94°) and inertness of the sulfur atom make it a poorer model for the substrate. The absence of a hydrogen bond between Gly344 and MTA allows the inhibitor more freedom in the active site that is revealed in the different geometry of the hydrogen bonds formed by the carboxylate group.

The close stacking (~3 Å) of the MTA sulfur atom and the PCA pyrrole ring over the O(4), C(4), C(4A) and N(5) portion of the flavin ring probably promotes the strong electronic interactions between the groups involved in the charge transfer interactions. Similar interactions occur between DAAO and OAB, which also form a charge transfer complex [24]. In the latter case, the plane of the benzene ring is parallel to the flavin ring plane and about 3–3.2 Å above it, with the amino nitrogen lying above the C(4)–C(4a) bond, thereby facilitating orbital overlap between unoccupied π-orbitals of the flavin ring and occupied π-orbitals of the OAB.

The inhibitors bind to MSOX facing the opposite direction from that observed for the benzoate inhibitors in DAAO [17,24]. The carboxylate of the benzoate in DAAO is hydrogen bonded to arginine and tyrosine sidechains that structurally align with Tyr317 and Tyr254, respectively, in MSOX. Although the two tyrosine residues in MSOX seem capable of binding inhibitor or substrate, Arg52 and Lys348 create a better binding site that structurally aligns with a glutamine and a threonine, respectively, in DAAO. This illustrates the divergence in the mode of catalytic activity of these two structurally related enzymes.

The pyrrole nitrogen of PCA and the sulfur of MTA, which both correspond to the nitrogen of the substrate, are positioned above C(4a) of the flavin ring. The methyl of MTA and the corresponding C(5) atom of PCA are positioned over N(5) of the flavin and close to His269 (3.3–3.7 Å) indicating that this histidine is a likely candidate for an active-site base. DAAO contains no basic residues in its active site.

Discussion

Enzyme catalysis

A hydrogen atom abstraction mechanism involving an amino acid radical as H• acceptor [25] can be ruled out for MSOX, as judged by electron paramagnetic resonance studies with the resting enzyme (R Hille and MSJ, unpublished results). Based on (bio)chemical precedent, sarcosine oxidation by MSOX may occur via a single electron transfer mechanism, a polar mechanism involving a covalent flavin-substrate 4a-adduct or a hydride transfer [26–30]. All three mechanisms are compatible with a model for the MSOX–sarcosine complex based on the structural data obtained for the MSOX–inhibitor complexes (see Figure 5b), even the latter two mechanisms, which have significant geometric constraints. Thus, the methyl group of sarcosine is predicted to be directly above N(5) of the flavin ring, suitably positioned for hydride transfer. Similarly, the amine nitrogen of sarcosine would be positioned above C(4a) of the flavin, as required for adduct formation in the polar mechanism (see Scheme 1 in Figure 6a). A water molecule near the *si* face of the flavin ring that forms a hydrogen bond to N(5) (3.0 Å), in conjunction with the putative PRS (see Figure 1a), could act as the general acid required for adduct formation (the next closest proton donor, the hydroxyl group of Tyr254, is 4.4–4.8 Å from N(5)). His269 is appropriately positioned to act as the base in the second step of the polar mechanism when the adduct must lose a proton from the substrate *N*-methyl group and undergo concomitant rearrangement to yield dihydroFAD and iminium product. In the single electron transfer mechanism (see Scheme 2 in Figure 6b), one electron transfer from the substrate amino group generates a flavin anion–amine cation radical pair. His269 could act as the base in the second step of the single electron transfer mechanism, abstracting a proton from the amine radical cation (pK_a ~ 8–10 [31,32]) to yield a carbon-centered radical. The carbon-centered radical undergoes a second one-electron transfer, forming iminium product and flavohydroquinone in a step that requires proton transfer to N(5). The water molecule near N(5) could act as the immediate proton donor and then accept a replacement proton from the PRS.

Figure 6

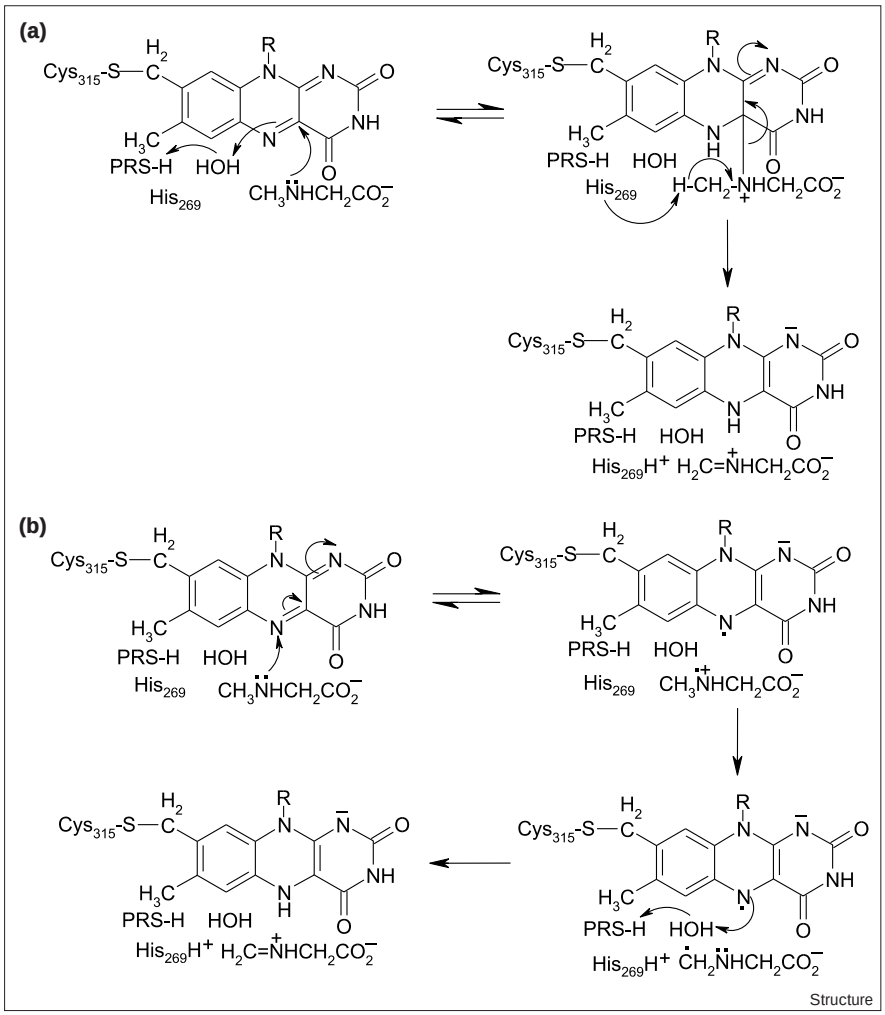

Possible mechanisms for sarcosine oxidation. The polar and single electron transfer mechanisms are shown in (**a**) Scheme I and (**b**) Scheme II, respectively. The hydride transfer mechanism is not shown.

Covalent flavinylation

The precise steps in the biosynthesis of flavoenzymes containing covalently bound flavin remain unknown but are likely to involve initial interaction of FAD with the apoprotein to yield a noncovalent intermediate, followed by covalent attachment in an apparently autocatalytic reaction [33–39]. By analogy with the mechanisms postulated for the covalent attachment of histidyl and tyrosyl residues to the 8α-methyl group of FAD in 6-hydroxy-D-nicotine oxidase and *p*-cresol methylhydroxylase (PCMH), respectively [36,37], one can envision that covalent flavinylation of MSOX occurs via initial flavin tautomerization to yield an electrophilic iminoquinone methide (Scheme III, Figure 7). The ε-amino group of Lys348 in MSOX is 2.8 Å from the C(2) carbonyl oxygen of the isoalloxazine ring. The positive end of a helix dipole (αF4) also points toward the same carbonyl oxygen. Both are ideally positioned to facilitate the development of negative charge at the N(1)–C(2) = O(2) locus during tautomerization. In a second step, the nucleophilic addition of Cys315 thiolate to the flavin iminoquinone methide generates the (8α–S-cysteinyl)-1,5-dihydroFAD anion. A base is needed to act as a proton acceptor from the 8α-methyl group of FAD during tautomerization and possibly to generate the reactive thiolate form of Cys315. Alternatively, the thiolate form of Cys315 may be stabilized by ion-pair formation with the nearby (3.8 Å) guanidinium group of Arg49. The closest base, His45, is nearer to the sulfur of Cys315 (4.7 Å) than the 8α-methyl group of FAD (6.5 Å). Given this scenario, the Cys315 thiolate may extract one of the protons from the 8α-methyl group and then transfer the proton to His45. It is also conceivable that His45 might be closer to the 8α-methyl group prior to covalent coupling. The water molecule that forms a hydrogen bond to N(5), in conjunction with the putative PRS (see Figure 1a), or Tyr254 could act as the proton donor during formation of the reduced covalent flavin. In the final step, the latter is oxidized by molecular oxygen.

Figure 7

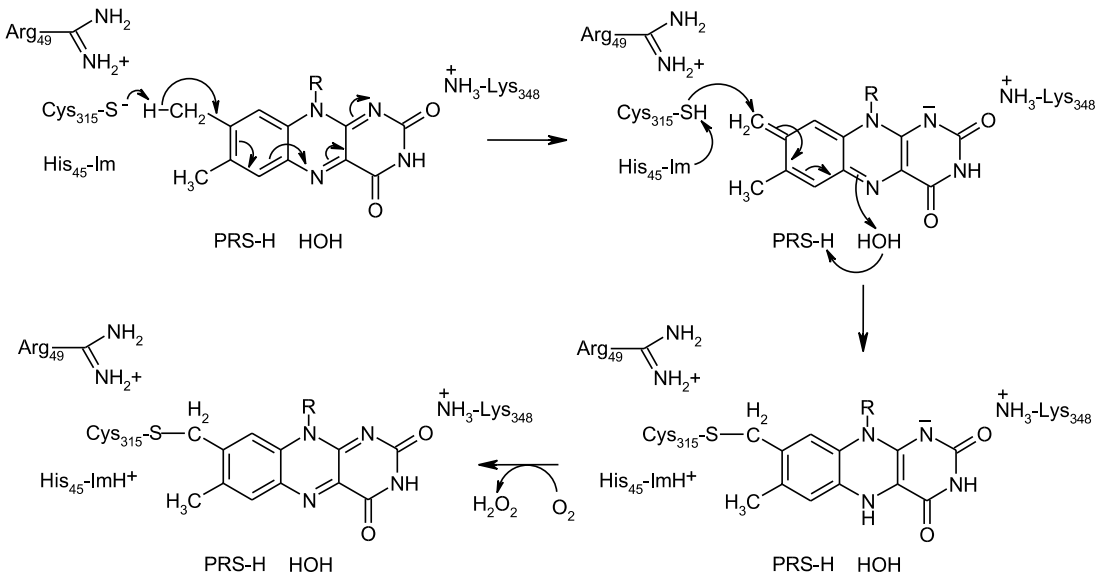

Proposed mechanism for covalent flavinylation in MSOX (Scheme III).

In addition to MSOX, four structures are known for enzymes with covalently bound flavin: PCMH [37]; vanillyl-alcohol oxidase (VAO) [40]; flavocytochrome *c* sulfide reductase (FCSD) [41]; and trimethylamine dehydrogenase (TMADH) [35]. All are flavinylated at the 8α position of the flavin except for TMADH. The mechanism proposed for covalent flavinylation of TMADH at C(6) [35], however, is similar to that envisioned for attachment at the 8α position. As observed for MSOX, these four proteins have centers of strong positive charge (helix dipole or a positive sidechain) near the flavin O(2) that could facilitate flavin tautomerization, except that both elements are present in MSOX (Table 2). The closest potential donors for protonation of N(5) are acidic sidechains in PCMH, VAO and FCSD (~3.5–5 Å) or a peptide amide in TMADH (3.9 Å) versus a water molecule (3.0 Å) and the PRS or Tyr254 (4.5 Å) in MSOX. None of the five proteins contains a nearby (≤ 4.8 Å) basic sidechain that could more effectively abstract a proton from flavin C(8α) or C(6), as compared with the attacking protein sidechain itself which forms the covalent bond (Table 2). For removal of a proton from the attacking protein nucleophile, there are potential active-site bases 4.4–5.6 Å from the sidechain in all five proteins. In addition, there is a nearby arginine in FCSD (Arg168) that could help stabilize the deprotonated form of attacking cysteine sidechain, similar to the role suggested for Arg49 in MSOX. It should be noted that the distances presented in Table 2 apply to the covalently flavinylated proteins and that the conformations of their precursors may differ.

Table 2

Electrostatic and/or sidechain interactions at various sites on the flavin ring that may be important for covalent flavinylation.

Protein	N1/O2 locus (Å)	N5 (Å)	Flavin C8α or C6 atom (Å)*†	Protein ligand atom (Å)†
MSOX	Lys348–O2 (2.8) and helix dipole	Tyr254 (4.5) and proton relay system	His45 ND1–C8α (6.5)	His45 ND1–Cys315 SG (4.7)
FCSD	Helix dipole only	Glu167 (4.8)	Arg168 NH1–C8α (5.5)	Arg168 NH1–Cys42 SG (5.1)
PCMH	Arg near O2 (3.0)	Glu380 (4.0)	Asp440 OD1–C8α (6.0)	Asp440 OD1–Tyr384 OH (5.2)
VAO	Arg near O2 (2.7)	Asp170 (3.4)	His61 ND1–C8α (5.2)	His61 ND1–His422 NE2 (4.4)
TMADH	Arg222 O2 (2.7)	Cys30 amide (2.9)	His29 ND1–C6 (4.8)	His29 ND1–Cys30 SG (5.6)

*These possible active-site bases do not include the covalent nucleophile. †The distances reflect the protein conformation in the covalently flavinylated form.

Figure 8

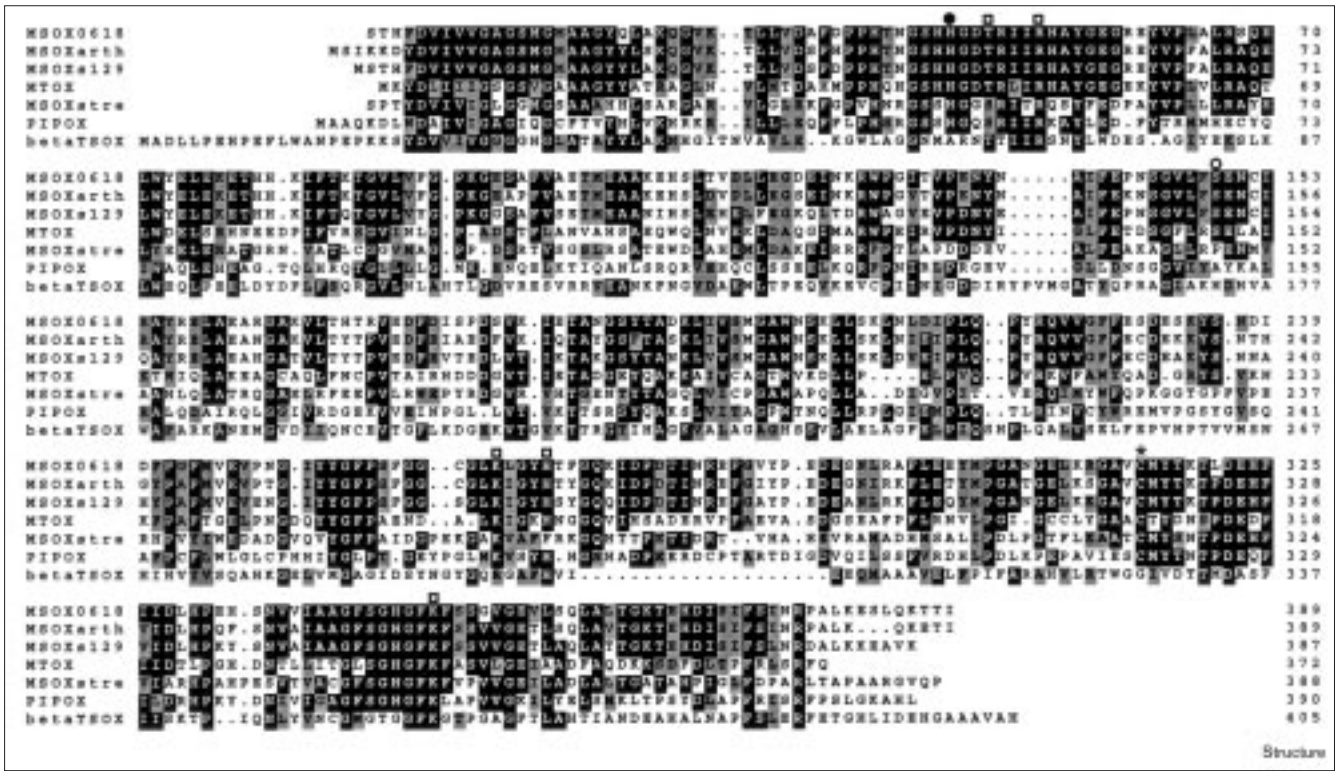

Multiple sequence alignment of MSOX from various sources – *Bacillus* sp. *B-0618* (MSOX0618); *Arthrobacter TE-1826* (MSOXarth); *Bacillus* sp. *NS-129* (MSOXs129); *Streptomyces* sp. *KB210-8SY* (MSOXstre) – plus MTOX from *E. coli*, PIPOX from rabbit and the β subunit of TSOX from *Corynebacterium* sp. *P-1* (betaTSOX). The covalent flavin attachment site in MSOX0618 is marked by an asterisk. The histidine and serine in MSOX0618 that align with the histidine covalent flavin attachment sites in SDH and betaTSOX are marked by a filled circle and an open circle, respectively. Putative catalytic residues in MSOX0618 are marked by open squares.

Homology of MSOX with other amine oxidoreductases

The closest homologs of MSOX are MTOX (42 kDa) from *E. coli* and mammalian PIPOX (44 kDa) as judged by overall sequence identity (43% and 30%, respectively) and by the conservation of residues at or near the active site (see Figure 8). Despite this similarity, sarcosine is a very poor substrate for MTOX, which exhibits a preference for aromatic or large aliphatic *N*-methyl amino acids [3] (P Khanna and MSJ, unpublished results). Structural and sequence data suggest that substitution of only one or two active-site residues (e.g. Met245 in MSOX → Thr238 in MTOX) may account for the observed difference in substrate specificity of MSOX and MTOX. MTOX and PIPOX contain a conserved cysteine that aligns with the covalent flavin attachment site in MSOX. Although the nature of the covalent flavin in PIPOX is unknown, MTOX has recently been found to contain 8α–(S-cysteinyl)FAD (MAW, P Khanna and MSJ, unpublished results). The observed homology of MTOX and PIPOX with MSOX suggests that these enzymes will exhibit both structural and mechanistic similarity to MSOX.

Similar to MSOXs, TSOXs are inducible bacterial enzymes but are the most complicated members of this family. TSOXs contain noncovalently bound FAD and NAD^+ and covalently bound flavin mononucleotide (FMN) (8α–(N^3-histidyl)FMN) that is attached to a histidyl residue in the β subunit (βTSOX; 44 kDa) [1,42–44]. βTSOX exhibits modest sequence homology (23% identity) with MSOX. Despite the modest sequence homology, all of the residues implicated in MSOX catalysis are conserved in βTSOX, including the two residues that bind the substrate carboxylate (Figure 8). The observed conservation of putative catalytic residues in βTSOX strongly suggests that this subunit binds FAD. This deduction is consistent with the presence of a single binding site for sarcosine near FAD that serves as the input site for electrons [45] and other observations that indicate that the covalent FMN is bound at an interface between βTSOX and another subunit (M Eschenbrenner and MSJ, unpublished results). The covalent FMN attachment site in βTSOX aligns with Ser149 in MSOX (Figure 8). The hydroxyl group of Ser149 in MSOX is located in a small depression on the protein surface, above the *si* face of

the FAD ring and about 8 Å from N(5). This places Ser149 on the side of the protein just opposite to the entry channel leading to the substrate-binding cavity on the *re* face of the FAD ring.

SDH (100 kDa) is a monomeric, mitochondrial matrix protein containing covalently bound FAD (8α–(N^3-histidyl)FAD) [46,47]. The putative covalent flavin attachment site in human SDH (His108) is located in the N-terminal half of the protein (M Eschenbrenner and MSJ, unpublished results), a region that exhibits modest sequence homology with MSOX (20% identity) and βTSOX (25% identity). SDH exhibits 35% identity with DMGDH, a very similar mitochondrial enzyme [4,8,9, 46–48] (M Eschenbrenner and MSJ, unpublished results). His108 in human SDH and the known covalent flavin attachment site in DMGDH [4] align with a conserved histidine in MSOX (His45), MTOX and PIPOX. His45 in MSOX is spatially near the covalent flavin attachment site at Cys315 and may play a role in covalent flavinylation (Scheme III, Figure 7). None of the residues in MSOX that are likely to bind sarcosine or participate in its oxidation, however, is conserved in SDH, whereas all are conserved in βTSOX. Structural and biochemical characterization of SDH and DMGDH are needed to clarify their relationship to MSOX and other more closely related members of this amine oxidoreductase family.

Biological implications

The crystal structure of monomeric sarcosine oxidase (MSOX) reported in this paper is the first structure for any member of a recently recognized family of bacterial and mammalian enzymes that oxidize secondary or tertiary amino acids and contain covalently bound flavin. The structure of free MSOX and the enzyme–inhibitor complexes provide insight into the possible mechanism of covalent flavin attachment and sarcosine oxidation, respectively. MSOX is unique among known flavoprotein structures because of its highly basic flavin environment, a feature likely to raise the flavin redox potential. The electropositive flavin environment in MSOX is opposite to that found in flavodoxin, where the redox potential of the neutral flavin radical/hydroquinone anion is very low owing, in part, to unfavorable electrostatic interactions between the flavin hydroquinone anion and the surrounding acidic residues [49–51].

The structure of MSOX is likely to provide a paradigm for other members of this amine oxidoreductase family. Pipecolate oxidase (PIPOX) and *N*-methyltryptophan oxidase (MTOX) are likely to exhibit close structural and mechanistic similarity to MSOX and contain flavin adenine dinucleotide (FAD) covalently attached to a cysteine residue near the C terminus. The β subunit of heterotetrameric sarcosine oxidase (TSOX) is likely to contain sites for the noncovalent binding of FAD and sarcosine and exhibit overall structural homology with MSOX, PIPOX and MTOX. Significant differences are expected, however, in the details of the FAD environment in TSOX and the mechanism of oxygen reduction, which involves interflavin electron transfer to a covalently bound flavin mononucleotide (FMN) that probably lies at the interface between the β subunit of TSOX and another subunit.

Although MSOX and mammalian monoamine oxidase do not exhibit sequence homology, these enzymes catalyze similar amine oxidation reactions, contain an N-terminal ADP-binding motif and a C-terminal attachment site for 8α–S-cysteinyl FAD. The mechanism of covalent flavin attachment in MSOX may provide a model for the reaction with monoamine oxidase for which no structural data are available.

Materials and methods

Enzyme preparation

Details of enzyme expression and isolation will be described elsewhere. Briefly, MSOX from *Bacillus* sp. *B-0618* [11] was expressed under the control of the *lac* promoter in *E. coli DH1* or *E. coli DL41* (a methionine-dependent strain), for the preparation of unsubstituted or selenomethionine-substituted enzyme, respectively. Cells were transformed using plasmid pMAW, a derivative of pOXI103, which was a gift from Masanori Sugiyama (Institute of Pharmaceutical Sciences, Faculty of Medicine, Hiroshima University). Transformed *E. coli DL41* cells were grown in the presence of selenomethionine, similar to the conditions described by Yang *et al.* [52]. MSOX was purified from crude cell lysates by ammonium sulfate fractionation and ion exchange chromatography.

Crystallization and data collection

Crystals of native and selenomethionine MSOX were obtained by hanging or sitting-drop vapor diffusion methods at 25°C, by mixing equal volumes of the protein solution (7 mg/ml in 20 mM Tris buffer, pH 8.0) and a reservoir containing 2.1 M Na/K phosphate buffer, pH 6.7. The native crystals are monoclinic, space group $P2_1$, with cell dimensions a = 72.6 Å, b = 69.6 Å, c = 74.1 Å and β = 94.3°. The selenomethionine crystals are isomorphous with the native, with mean changes in cell parameters of 0.1%. The crystals were frozen after brief exposure to a cryoprotecting solution containing 2.1 M Na/K phosphate buffer (pH 6.7) and 25% (v/v) glycerol.

MAD data were collected at beamline 19ID at the Advanced Photon Source, Argonne, IL. Data processing was carried out using the HKL package [53]. All MAD data were collected from a single selenomethionine MSOX crystal, which was frozen at 100K. Data sets were collected at four wavelengths at or near the K absorption edge of selenium (Table 1). Wavelengths were selected on the basis of an X-ray fluorescence spectrum collected directly from the crystal: edge (0.9794 Å) was optimized for f′; peak (0.9792 Å) was at maximal f″; low (1.0679 Å) and high (0.9392 Å) were recorded to obtain the dispersive differences. Because of the alignment of the crystal in the cryo-loop, an inverse beam experiment was performed in which, at each energy, data were recorded over a range of Omega at Chi = 0, Kappa = 0 and fixed Phi and again at Phi + 80.

After the structure was solved, the following 2.0 Å resolution data sets were collected at 100K on laboratory X-ray sources: a native data set with an R-AxisIV image plate system; a selenomethionine crystal soaked in (methylthio)acetic acid (20 mM for 1.5 h) with an R-AxisII image plate system and a selenomethionine crystal soaked in pyrrole-2-carboxylic acid (10 mM for 1 h) with an R-AxisIV image plate system. The isomorphous crystals showed mean changes in cell parameters of 0.3% and

maximum changes of 0.5%. All data sets were processed using the program DENZO/SCALEPACK [53]. Statistics of the data collections are shown in Table 1.

MAD analysis

The MAD data were combined with the program MADMRG [54] and analyzed using HEAVY and SOLVE [55,56]. From Patterson maps calculated with the anomalous differences and with the dispersive differences, 14 selenium sites were found in the asymmetric unit, indicating the presence of two molecules per asymmetric unit. Visual analysis of the heavy-atom coordinates revealed the presence of a local twofold axis that is approximately parallel to the crystallographic b axis relating the two molecules in the asymmetric unit. This allowed us to establish the NCS operator relating the two molecules using the program LSQKAB [57].

The selenium parameters were refined with the maximum-likelihood program SHARP [58], and solvent flattened using a solvent content of 42%. The resulting electron-density map was averaged about the NCS twofold axis with further solvent flattening, using DM [57]. Masks were calculated with NCSMASK [57]. The final figure of merit was 0.92 to 2.0 Å.

The quality of the experimental map was exceptionally good as expected from the phasing statistics (Figure 1a). All mainchain and sidechains except for a few terminal residues could readily be modeled in the electron density, using the program TURBO [59].

Refinement and quality of the models

The selenomethionine MSOX model was subjected to simulated annealing refinement with X-PLOR [60], using tightly restrained NCS. This was followed by several rounds of positional and temperature factor refinement with loose NCS restraints, combined with manual rebuilding. About 200 water molecules were added. One of the water molecules in each subunit, which interacts with an oxygen of the ribityl chain, corresponded to strong electron density, refines to a low B-factor (ca. 5 Å) and may be a metal ion. The final model consists of residues 1–385 for both molecules as there was no density for the remaining four residues. The refined selenomethionine structure without water was subjected to simulated annealing refinement against the native data set, followed by a refinement procedure similar to that employed with the selenomethionine structure. Difference density maps, $2F_o–F_c$, were calculated for the selenomethionine inhibitor-soaked data sets, followed by modeling of the inhibitor into the resulting density. The refinement statistics and quality of model indicators for all four structures are in Table 1.

Accession numbers

The coordinates of MSOX have been deposited with the Protein Data Bank with accession code 1B3M.

Acknowledgements

This work was supported by USPHS grants GM20530 (FSM) and GM31704 (MSJ). Use of the Argonne National Laboratory Structural Biology Center beamlines at the Advanced Photon Source was supported by the US Department of Energy, Basic Energy Sciences, Office of Energy Research, under contract number W-31-109-Eng-38. We thank Masanori Sugiyama for his generous gift of plasmid pOXI103.

References

1. Chlumsky, L.J., Zhang, L. & Jorns, M.S. (1995). Sequence analysis of sarcosine oxidase and nearby genes reveals homologies with key enzymes of folate one-carbon metabolism. *J. Biol. Chem.* 270, 18252-18259.
2. Reuber, B.E., Karl, C., Reimann, S.A., Mihalik, S.J. & Dodt, G. (1997). Cloning and functional expression of a mammalian gene for a peroxisomal sarcosine oxidase. *J. Biol. Chem.* 272, 6766-6776.
3. Koyama, Y. & Ohmori, H. (1996). Nucleotide sequence of the *Escherichia coli Sola* gene encoding a sarcosine oxidase-like protein and characterization of its product. *Gene* 181, 179-183.
4. Lang, H., Polster, M. & Brandsch, R. (1991). Rat liver dimethylglycine dehydrogenase: flavinylation of the enzyme in hepatocytes in primary culture and characterization of a cDNA clone. *Eur. J. Biochem.* 198, 793-799.
5. Kvalnes-Krick, K. & Jorns, M.S. (1991). Role of the covalent and noncovalent flavins in sarcosine oxidase. In *Chemistry and Biochemistry of Flavoenzymes* (Muller, F., ed), pp. 425-435, CRC Press, Inc., Boca Raton.
6. Gutierrez, M. & Delgado-Coello, B.A. (1989). Influence of pipecolic acid on the release and uptake of [^{3}H]-GABA from brain slices of mouse cerebral cortex. *Neurochem. Res.* 14, 405-408.
7. Ho, B. & Zabriskie, T.M. (1998). Epoxide derivatives of pipecolic acid and proline are inhibitors of pipecolate oxidase. *Bioorg. Med. Chem. Lett.* 8, 739-744.
8. Wittwer, A.J. & Wagner, C. (1981). Identification of the folate-binding proteins of rat liver mitochondria as dimethylglycine dehydrogenase and sarcosine dehydrogenase. Flavoprotein nature and enzymatic properties of the purified proteins. *J. Biol. Chem.* 256, 4109-4115.
9. Wittwer, A.J. & Wagner, C. (1981). Identification of the folate-binding proteins of rat liver mitochondria as dimethylglycine dehydrogenase and sarcosine dehydrogenase. Purification and folate-binding characteristics. *J. Biol. Chem.* 256, 4102-4108.
10. Yeo, E. & Wagner, C. (1994). Tissue distribution of glycine N-methyltransferase, a major folate-binding protein of liver. *Proc. Natl Acad. Sci. USA* 91, 210-214.
11. Suzuki, K., Sagai, H., Imamura, S. & Sugiyama, M. (1994). Cloning, sequencing, and overexpression in *Escherichia coli* of a sarcosine oxidase-encoding gene linked to the *Bacillus* creatinase gene. *J. Ferm. Bioe.* 77, 231-234.
12. Wagner, M.A. & Jorns, M.S. (1997). Folate utilization by monomeric *versus* heterotetrameric sarcosine oxidases. *Arch. Biochem. Biophys.* 342, 176-181.
13. Hendrickson, W.A. & Ogata, C.M. (1997). Phase determination from multiwavelength amomalous diffraction measurements. *Methods Enzymol.* 276, 494-523.
14. Morris, A.L., MacArthur, M.W., Hutchinson, E.G. & Thornton, J.M. (1992). Stereochemical quality of protein structure coordinates. *Proteins* 12, 345-364.
15. Schreuder, H.A., *et al.*, & Drenth, J. (1989). Crystal structure of the p-hydroxybenzoate hydroxylase-substrate complex refined at 1.9 Å resolution. *J. Mol. Biol.* 208, 679-696.
16. Karplus, P.A. & Schulz, G.E. (1987). Refined structure of glutathione reductase at 1.54 Å resolution. *J. Mol. Biol.* 195, 701-729.
17. Mattevi, A., *et al.*, & Curti, B. (1996). Crystal structure of D-amino acid oxidase: a case of active site mirror-image convergent evolution with flavocytochrome b_2. *Proc. Natl Acad. Sci. USA* 93, 7496-7501.
18. Mizutani, H., *et al.*, & Miura, R. (1996). Three-dimensional structure of porcine kidney D-amino acid oxidase at 3.0 Å resolution. *J. Biochem.* 120, 14-17.
19. Li, J., Vrielink, A., Brick, P. & Blow, D.M. (1993). Crystal structure of cholesterol oxidase complexed with a steroid substrate: implications for flavin adenine dinucleotide dependent alcohol oxidases. *Biochemistry* 32, 11507-11515.
20. Hecht, H.J., Kalisz, H.M., Hendle, J., Schmid, R.D. & Schomburg, D. (1993). Crystal structure of glucose oxidase from *Aspergillus niger* refined at 2.3 Å resolution. *J. Mol. Biol.* 229, 153-172.
21. Enroth, C., Neujahr, H., Schneider, G. & Lindqvist, Y. (1998). The crystal structure of phenol hydroxylase in complex with FAD and phenol provides evidence for a concerted conformational change in the enzyme and its cofactor during catalysis. *Structure* 6, 605-617.
22. Holm, L. & Sander, C. (1993). Protein structure comparison by alignment of distance matrices. *J. Mol. Biol.* 233, 123-138.
23. Raibekas, A.A., Ramsey, A.J. & Jorns, M.S. (1993). Properties of a high-potential flavin analogue and its use as an active site probe with clostridial flavodoxin. *Biochemistry* 32, 4420-4429.
24. Miura, R., *et al.*, & Hirotsu K. (1997). Structural and mechanistic studies on D-amino acid oxidase–substrate complex: implications of the crystal structure of enzyme substrate analog complex. *J. Biochem.* 122, 825-833.
25. Walker, M.C. & Edmondson, D.E. (1994). Structure-activity relationships in the oxidation of benzylamine analogues by bovine liver mitochondrial monoamine oxidase B. *Biochemistry.* 33, 7088-7098.
26. Silverman, R.B. (1995). Radical ideas about monoamine oxidase. *Account. Chem. Res.* 28, 335-342.
27. Kim, J.M., Bogdan, M.A. & Mariano, P.S. (1993). Mechanistic analysis of the 3-methyllumiflavin-promoted oxidative deamination of benzylamine – a potential model for monoamine oxidase catalysis. *J. Am. Chem. Soc.* 115, 10591-10595.
28. Kim, J.M., Hoegy, S.E. & Mariano, P.S. (1995). Flavin chemical models for monoamine oxidase inactivation by cyclopropylamines, alpha-silylamines, and hydrazines. *J. Am. Chem. Soc.* 117, 100-105.

29. Thompson, J. & Donkersloot, J.A. (1992). N-Carboxyalkyl)amino acids: occurrence, synthesis and functions. *Ann. Rev. Biochem.* 61, 517-557.
30. Yoneda, F., Sakuma, Y. & Kadokawa, Y. (1979). Oxidation of amines to carbonyl compounds by pyrimido[4,5-b]quinoline-2,4(3H,10H)-dione (5-deazaflavin). *Chem. Lett.* 1469-1468.
31. Dinnocenzo, J.P. & Banach, T.E. (1989). Deprotonation of tertiary amine cation radical. A direct experimental approach. *J. Am. Chem. Soc.* 111, 8646-8653.
32. Das, S. & von Sonntag, C.Z. (1986). The oxidation of trimethylamine by OH radicals in aqueous solution as studied by pulse radiolysis, electron spin resonance and product analysis. The reactions of the alkylamine radical cation, the aminoalkyl radical and the protonated aminoalkyl radical. *Z. Naturforsch. B* 41, 505-513.
33. Nagursky, H., Bichler, V. & Brandsch, R. (1988). Phosphoenolpyruvate dependent flavinylation of 6-hydroxy-D-nicotine oxidase. *Eur. J. Biochem.* 177, 319-325.
34. Brandsch, R. & Bichler, V. (1989). Covalent factor binding to flavoenzymes requires specific effectors. *Eur. J. Biochem.* 182, 125-128.
35. Scrutton, N.S., Packman, L.C., Mathews, F.S., Rohlfs, R.J. & Hille, R. (1994). Assembly of redox centers in the trimethylamine dehydrogenase of bacterium W(3)A(1) - Properties of the wild-type enzyme and a C30A mutant expressed from a cloned gene in *Escherichia coli*. *J. Biol. Chem.* 269, 13942-13950.
36. Brandsch, R. & Bichler, V. (1991). Autoflavinylation of apo6-hydroxy-D-nicotine oxidase. *J. Biol. Chem.* 266, 19056-19062.
37. Kim, J., *et al*., & McIntire, W.S. (1995). The cytochrome subunit is necessary for covalent attachment of the flavoprotein subunit of p-cresol methylhydroxylase. *J. Biol. Chem.* 270, 31202-31209.
38. Chlumsky, L.J., Zhang, L.N., Ramsey, A.J. & Jorns, M.S. (1993). Preparation and properties of recombinant corynebacterial sarcosine oxidase: evidence for posttranslational modification during turnover with sarcosine. *Biochemistry* 32, 11132-11142.
39. Zhou, B.P., Wu, B., Kwan, S.W. & Abell, C.W. (1998). Characterization of a highly conserved FAD-binding site in human monoamine oxidase B. *J. Biol. Chem.* 273, 14862-14868.
40. Mattevi, A., Fraaije, M.W., Mozzarelli, A., Olivi, L., Coda, A. & Vanberkel, W.J.H. (1997). Crystal structures and inhibitor binding in the octameric flavoenzyme vanillyl-alcohol oxidase – the shape of the active-site cavity controls substrate specificity. *Structure* 5, 907-920.
41. Chen, Z.-w., *et al*., & Mathews, F.S. (1994). The structure of flavocytochrome c sulfide dehydrogenase from a purple phototrophic bacterium. *Science* 266, 430-432.
42. Willie, A. & Jorns, M.S. (1995). Discovery of a third coenzyme in sarcosine oxidase. *Biochemistry* 34, 16703-16707.
43. Willie, A., Edmondson, D.E. & Jorns, M.S. (1996). Sarcosine oxidase contains a novel covalently bound FMN. *Biochemistry* 35, 5292-5299.
44. Chlumsky, L.J., Sturgess, A.W., Nieves, E. & Jorns, M.S. (1998). Identification of the covalent flavin attachment site in sarcosine oxidase. *Biochemistry* 37, 2089-2095.
45. Zeller, H.-D., Hille, R. & Jorns, M.S. (1989). Bacterial sarcosine oxidase: identification of novel substrates and a biradical reaction intermediate. *Biochemistry* 28, 5145-5154.
46. Cook, R.J., Misono, K.S. & Wagner, C. (1984). Identification of the covalently bound flavin of dimethylglycine dehydrogenase and sarcosine dehydrogenase from rat liver mitochondria. *J. Biol. Chem.* 259, 12475-12480.
47. Porter, D.H., Cook, R.J. & Wagner, C. (1985). Enzymatic properties of dimethylglycine dehydrogenase and sarcosine dehydrogenase from rat liver. *Arch. Biochem. Biophys.* 243, 396-407.
48. Cook, R.J. & Wagner, C. (1986). Dimethylglycine dehydrogenase and sarcosine dehydrogenase: Mitochondrial folate-binding proteins from rat liver. *Methods Enzymol.* 122, 255-260.
49. Zhou, Z.M. & Swenson, R.P. (1995). Electrostatic effects of surface acidic amino acid residues on the oxidation-reduction potentials of the flavodoxin from *Desulfovibrio vulgaris* (Hildenborough). *Biochemistry* 34, 3183-3192.
50. Swenson, R.P. & Krey, G.D. (1994). Site-directed mutagenesis of tyrosine-98 in the flavodoxin from *Desulfovibrio* vulgaris (Hildenborough): regulation of oxidation-reduction properties of the bound FMN cofactor by aromatic, solvent, and electrostatic interactions. *Biochemistry* 33, 8505-8514.
51. Swenson, R.P. & Zhou, Z. (1997). Role of electrostatic interactions in the regulation of the one-electron reduction potentials in the *Desulfovibrio* flavodoxin. In *Flavins and Flavoproteins 1996.* (Stevenson, K.J., Massey, V., and Williams, C.H.J., eds), pp. 427-436, University of Calgary Press, Calgary.
52. Yang, W., Hendrickson, W.A., Kalman, E.T. & Crouch, R.J. (1990). Expression, purification and crystallization of natural and selenomethionyl recombinant ribonuclease H from *Escherichia coli*. *J. Biol. Chem.* 265, 13553-13559.
53. Otwinowski, Z. & Minor, W. (1997). Processing of X-ray diffraction data collected in oscillation mode. *Methods Enzymol.* 276, 307-326.
54. Terwilliger, T.C. (1994). MAD phasing: treatment of dispersive differences as isomorphous replacement information. *Acta Crystallogr. D* 50, 17-23.
55. Terwilliger, T.C., Kim, S.-H. & Eisenberg, D. (1987). Generalized method of determining heavy-atom positions using the difference Patterson function. *Acta Crystallogr. A* 43, 1-5.
56. Terwilliger, T.C. (1994). MAD phasing: Bayesian estimates of Fa. *Acta Crystallogr. D* 50, 11-16.
57. Collaborative Computational Project, Number 4 (1994). The CCP4 suite: programs for protein crystallography. *Acta Crystallogr. D* 50, 760-763.
58. La Fortelle, E. de, Irwin, J.J. & Bricogne, G. (1997). SHARP: a maximum-likelihood heavy-atom parameter refinement and phasing program for the MIR and MAD methods. In *Crystallographic Computing 7.* (Bourne, P. & Watenpaugh, K. eds).
59. Roussel, A. & Cambillau, C. (1991). TURBO-FRODO. In *Silicon Graphics Geometry Partners Directory 86*. Silicon Graphics, Mountain View, CA, USA.
60. Brünger, A.T. (1993). X-PLOR (version 3.1). In *Manual of a System for Crystallography and NMR*. Yale University, New Haven, Connecticut.
61. Kraulis, P.J. (1991). MOLSCRIPT: a program to produce both detailed and schematic plots of protein structures. *J. Appl. Crystallogr.* 24, 946-950.
62. Bacon, D.J. & Anderson, W.F. (1988). A fast algorithm for rendering space-filling model figures. *J. Mol. Graph.* 6, 219-220.
63. Merritt, E.A. & Murphy, M.E.P. (1994). Raster3D version 2.0 – a program for photorealistic molecular graphics. *Acta Crystallogr. D* 50, 869-873.
64. Nicholls, A., Sharp, K.A. & Honig, B. (1991). Protein folding and association: insights from the interfacial and thermodynamic properties of hydrocarbons. *Proteins* 11, 281-296.

Because *Structure with Folding & Design* operates a 'Continuous Publication System' for Research Papers, this paper has been published on the internet before being printed (accessed from http://biomednet.com/cbiology/str). For further information, see the explanation on the contents page.